Supplementary materials for

Oxygen ion pumping across atomically designed oxide heterointerfaces

Yongshun Wu†, Yang Zhang†, Jianbing Zhang, Yingjie Lyu, Cong Li, Sijie Wu, Meng Wang, Youwen Long, Tianxiang Nan, Di Yi, Qing He, Shuyun Zhou and Pu Yu*

This PDF includes

FIG S1-S10.

Reference

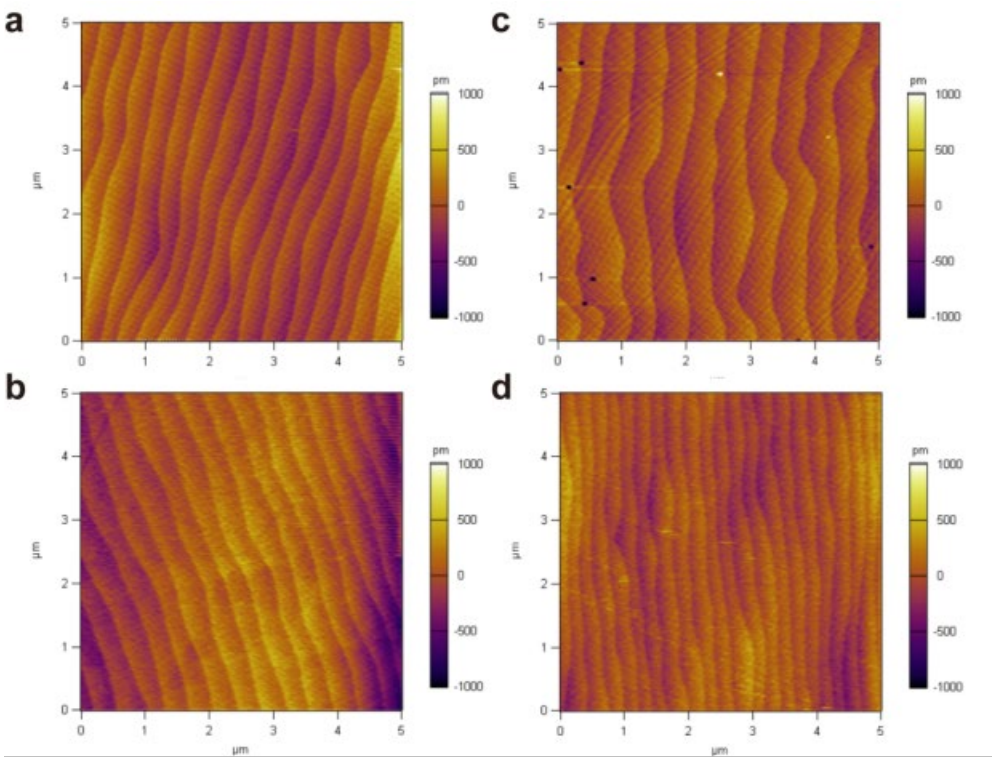

Figure S1. Topographic images of different heterostructures. Atomic force microscopy images of (**a**) the $SrTiO_3$ (STO) (001) substrate, (**b**) the $La_{0.7}Sr_{0.3}MnO_3/CaFeO_{2.5}$ (STO//LSMO/CFO) heterostructure, (**c**) the $CaFeO_{2.5}/La_{0.7}Sr_{0.3}MnO_3$ (STO//LSMO/CFO) heterostructure, and (**d**) the $La_{0.7}Sr_{0.3}MnO_3/CaFeO_{2.5}/La_{0.7}Sr_{0.3}MnO_3$ (LSMO/CFO/LSMO) heterostructure. All samples show atomically flat terraces as defined by the vicinal STO substrate, which affirm the layer-by-layer growth mode.

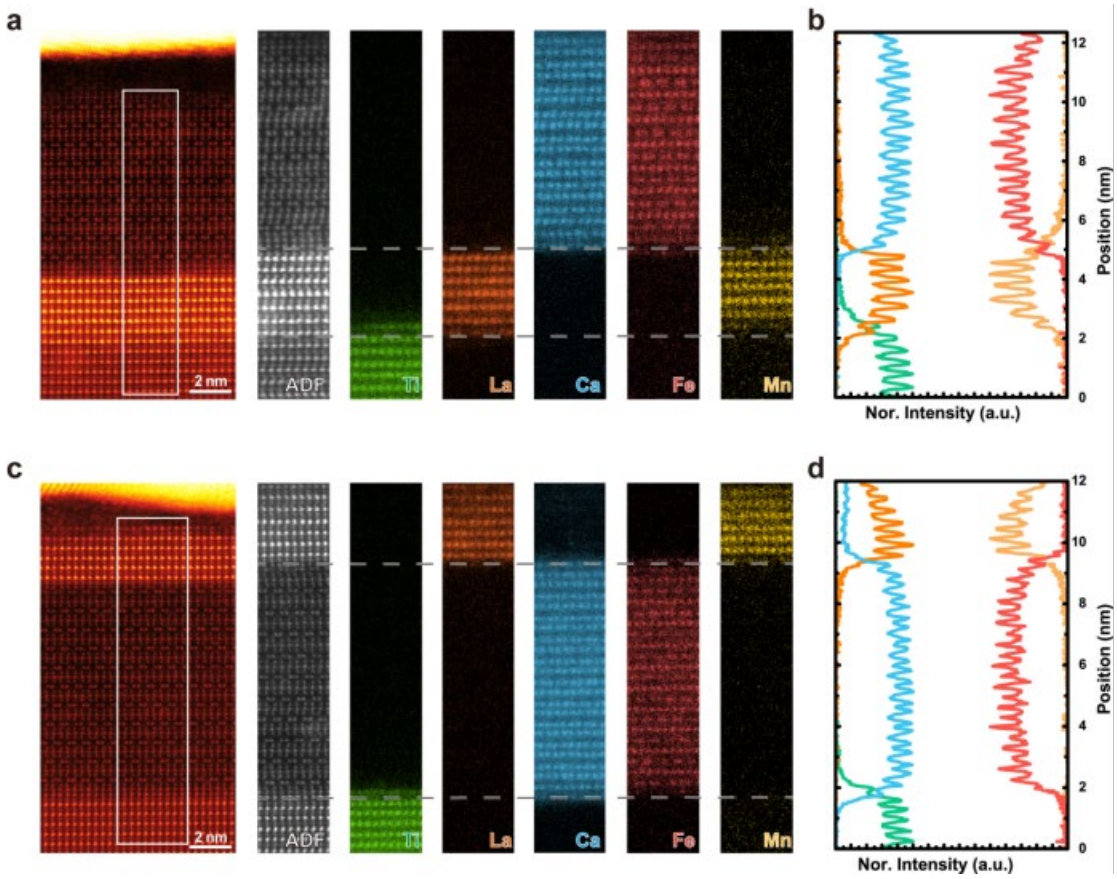

Figure S2. Extended high-resolution transmission electron microscopy (HRTEM) results. (**a**) HRTEM images of the STO//LSMO/CFO heterostructure. Left: High-angle annular dark field scanning (HAADF) images. Middle: Electron energy-loss spectroscopy (EELS) mapping of region marked by white rectangle in HAADF-STEM image. The ADF image is simultaneously recorded during EELS acquisition. The black dashed line represents the interface. (**b**) EELS signals of different elements extracted along the depth direction. **(c, d)** The corresponding HAADF-STEM image and EELS result of the STO//CFO/LSMO heterostructure.

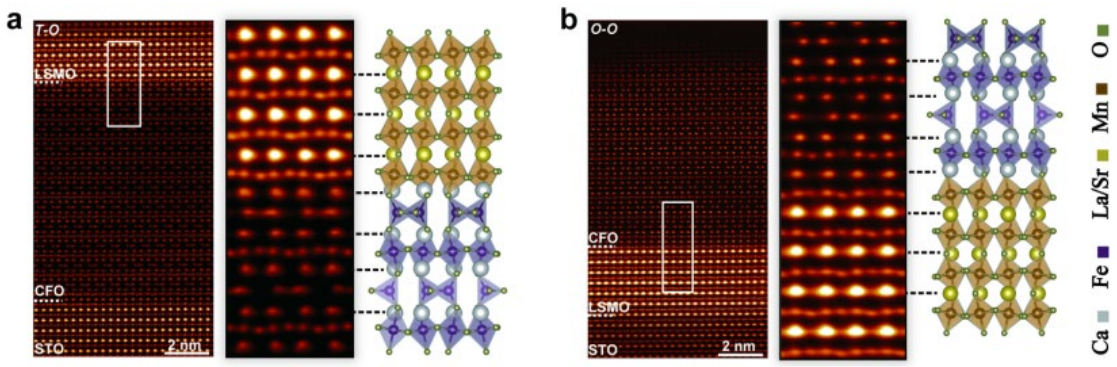

Figure S3. ABF-STEM images of **(a)** the T_d-O_h and **(b)** the O_h-O_h heterointerfaces, respectively. The left panel is the cross-sectional view of the heterostructures. The middle panel shows a zoom-in view across the interface of LSMO and CFO (the white square region). The right panel is the corresponding crystal schematics of the heterointerfaces.

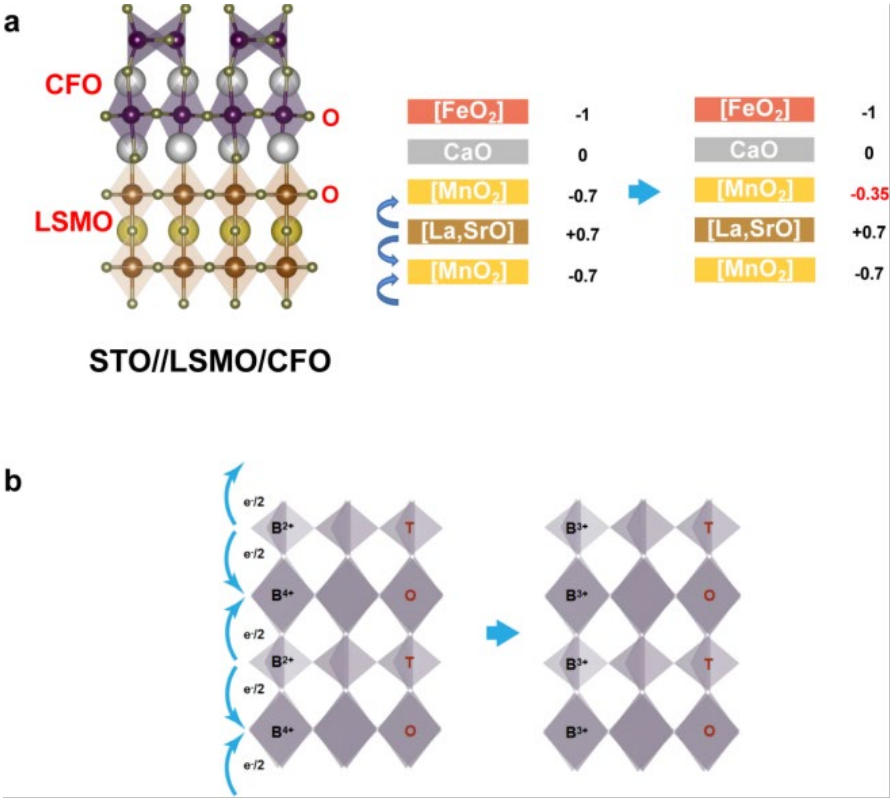

Figure S4. (a) Schematic illustration of "polar catastrophe" mechanism at the LSMO/CFO heterointerfaces. The charge mismatch at the interface formed by the charged LSMO atomic layers and the charge-neutral CaO layers could induces a polarity discontinuity [1-2] at the O_h-O_h heterointerfaces. To avoid the divergence of the electrostatic potential, a net charge transfer across the interface is developed, which would increase the valence state of Mn ions. We note that this is contradictory to the experimental observation with reduced valence state in Mn ions in such heterostructure (**Figures 2**e-f**)**. (**b**) Charge transfer between O_h-T_d sublayers within the brownmillerite structure. Since only Fe^{3+} ions were observed in the brownmillerite phase experimentally [3], we deduce that there is a strong charge transfer from the FeO_4 tetrahedra to the FeO_6 octahedra. Hence, the electron transfer from MnO_6 (LSMO layer) to FeO_6 octahedra (CFO layer) would further increase the valence state of Mn ions in O_h-O_h heterointerfaces. This is also opposite to the experimental result. With these studies, an alternative mechanism is highly demanded to account for the experimental results, which as we discussed in the manuscript is attributed to the oxygen ion migration across the heterointerface.

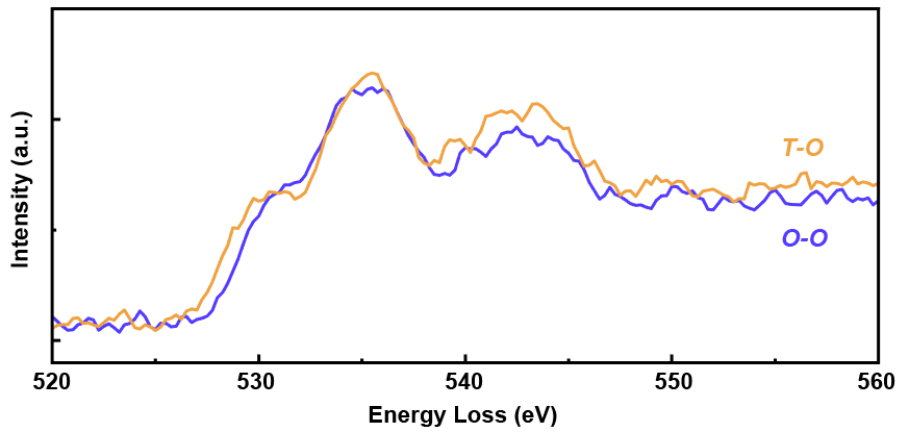

Figure S5. EELS spectra collected at oxygen *K*-edge for O_h-O_h (blue line) and T_d-O_h (yellow line) heterointerfaces, which are corresponding to the heterostructures of STO//LSMO/CFO and STO//CFO/LSMO, respectively.

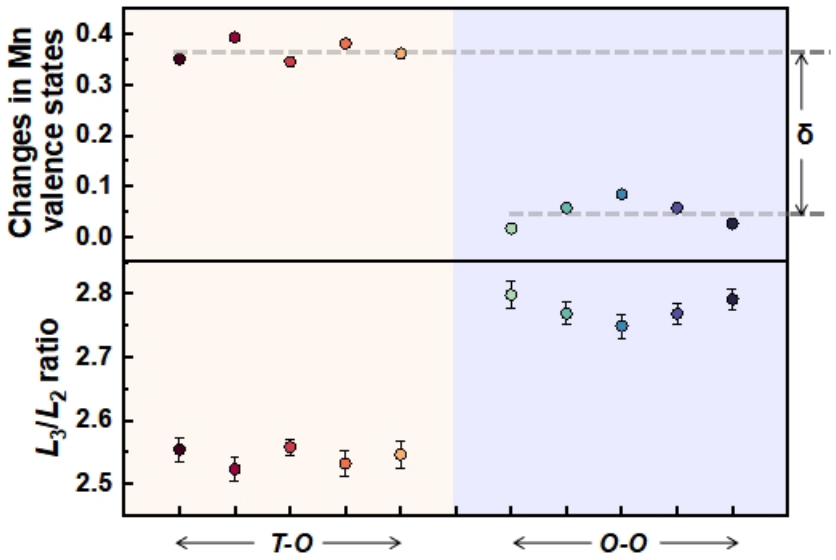

Figure S6. L_3/L_2 ratio derived from atomic-layer-dependent EELS signals measured at Mn $L_{3,2}$ edges for the O_h-O_h and T_d-O_h heterointerfaces and the resulting changes in Mn valence states [4]. The thickness of LSMO layers is 7 u.c. shown in this figure.

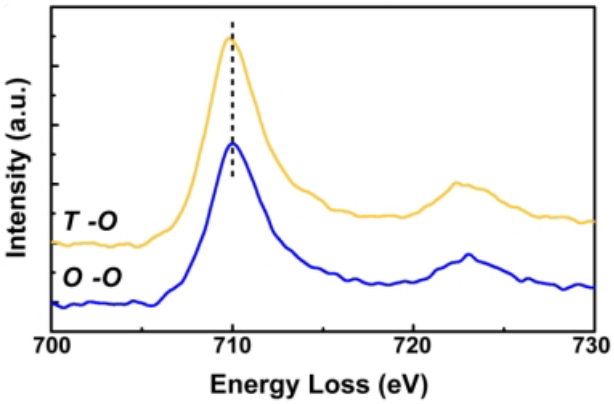

Figure S7. EELS spectra collected at Fe $L_{3,2}$ edges for O_h-O_h (blue line) and T_d-O_h (yellow line) heterointerfaces, which are corresponding to the heterostructures of STO//LSMO/CFO and STO//CFO/LSMO, respectively.

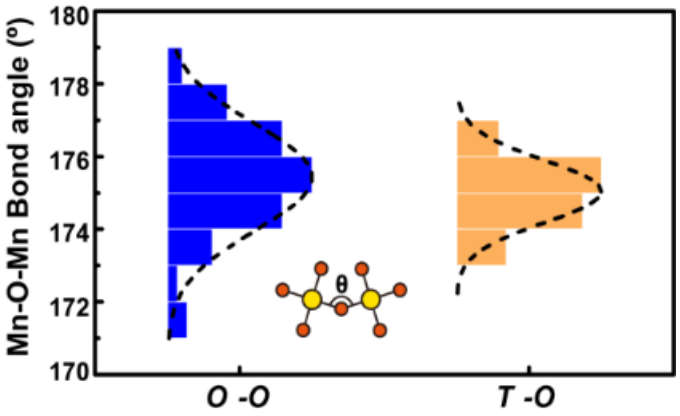

Figure S8. Analysis of the Mn-O-Mn bond-angle within LSMO layers for both O_h-O_h (blue) and T_d-O_h (yellow) heterointerfaces.

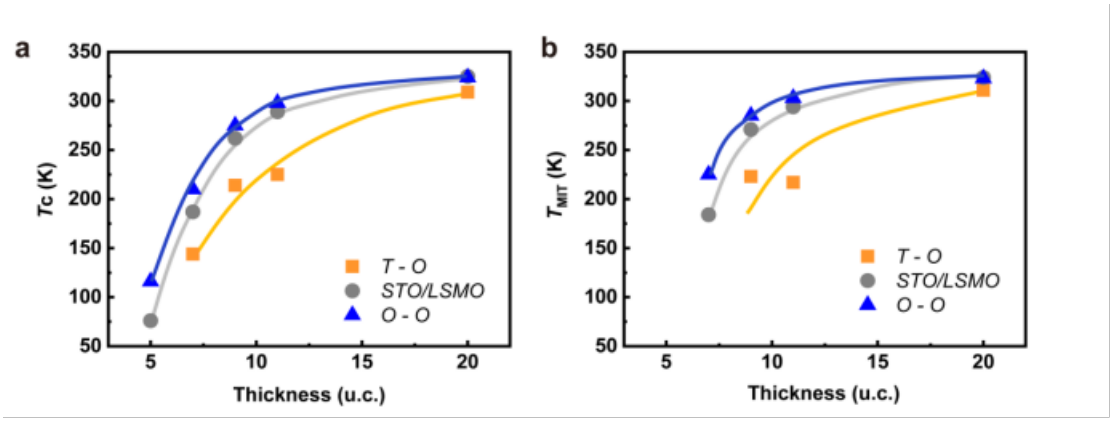

Figure S9. Thickness dependent (**a**) Curie temperature (T_C) and (**b**) metal-insulator transition temperature (T_{MIT}) of O_h-O_h (blue) and T_d-O_h (yellow) heterointerfaces. The data from STO//LSMO (gray) thin films were also measured as the reference.

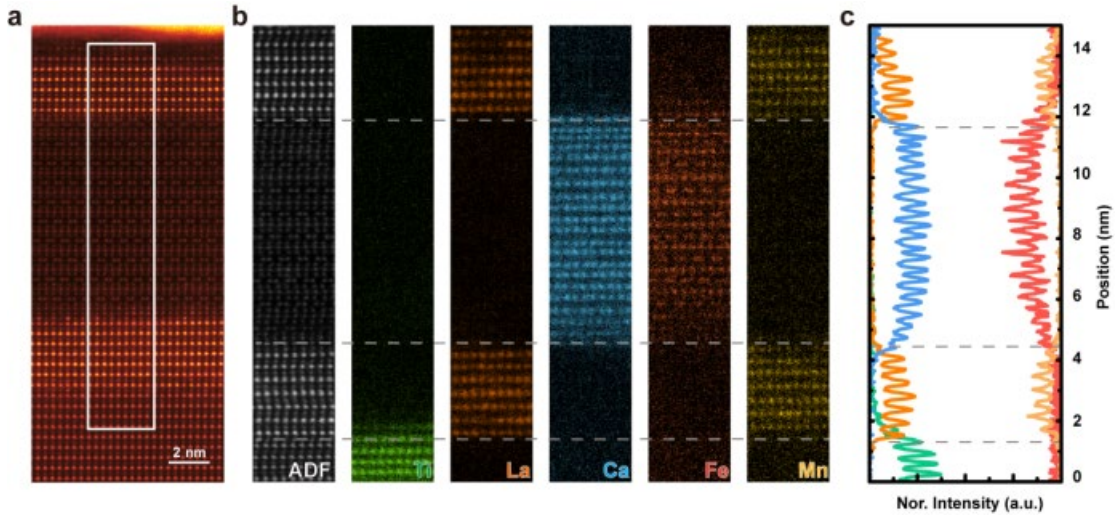

Figure S10. (**a**) HAADF images of STO//LSMO/CFO/LSMO tri-layer heterostructure. (**b**) Electron energy-loss spectroscopy (EELS) mapping of region marked by white rectangle in HAADF-STEM image. The ADF image is simultaneously recorded during EELS acquisition. The black dashed line represents the interface. (**c**) EELS signals of different elements extracted along the depth direction.

References:

[1] E. J. Guo, M. A. Roldan, T. Charlton, Z. Liao, Q. Zheng, H. Ambaye, A. Herklotz, Z. Gai, T. Z. Ward, H. N. Lee, M. R. Fitzsimmons, *Adv. Funct. Mater.* **2018**, *28*, 1800922.

[2] H. Boschker, J. Verbeeck, R. Egoavil, S. Bals, G. van Tendeloo, M. Huijben, E. P. Houwman, G. Koster, D. H. A. Blank, G. Rijnders, *Adv. Funct. Mater.* **2012**, *22*, 2235.

[3] A. Gloter, J. Ingrin, D. Bouchet, C. Colliex, *Physical Review B* **2000**, 61, 2587.

[4] M. Varela, M. P. Oxley, W. Luo, J. Tao, M. Watanabe, A. R. Lupini, S. T. Pantelides, S. J. Pennycook, *Phys. Rev. B* **2009**, 79, 085117.